

The roedderite–chayesite series from Spanish lamproites: crystal-chemical characterization

E. ALIETTI, M. F. BRIGATTI, S. CAPEDEI AND L. POPPI

Dipartimento di Scienze della Terra, Università di Modena, Via S. Eufemia, 19, I-41100 Modena, Italy

Abstract

Members of the roedderite–chayesite series in lamproites from Cancarix (SE Spain), crystallized from late magmatic residua under low P_{H_2O} , high temperature ($\sim 1100^\circ\text{C}$), oxidizing conditions. They exhibit the following main chemical variations: $0.14 \leq \text{Na} \leq 0.62$ atoms per formula unit (apfu); $0.80 \leq \text{K} \leq 1.00$ apfu; $2.97 \leq \text{Mg} \leq 4.33$ apfu; $0.00 \leq \text{Fe}^{2+} \leq 1.19$ apfu; $0.42 \leq \text{Fe}^{3+} \leq 0.87$ apfu; they are hexagonal ($10.120 \leq a \leq 10.135$ Å, $14.305 \leq c \leq 14.326$ Å), $P6/mcc$. The characteristic chemical substitution is: $\text{Fe}^{3+} + \square \rightleftharpoons \text{Fe}^{2+} + (\text{K} + \text{Na})^+$. Six crystal structures have been refined to $0.020 \leq R_{\text{obs}} \leq 0.026$. They have the osumilite/milarite-type structure, with Si entering the double tetrahedral $T1$ six-membered rings, and Mg and Fe entering both the ring-linking $T2$ tetrahedra, and the A octahedra. The 12-coordinated C site, located between two double rings of $T1$ tetrahedra, is occupied mainly by K and subordinately by Na. Furthermore, Na occupies the partially empty nine-fold coordinated B site which occurs both in the ideal ($z = 0$) and in a split-atom position along the c direction.

KEYWORDS: roedderite, chayesite, milarite group, lamproite, Cancarix, Spain.

Introduction

CHAYESITE $[\text{K}(\text{Mg}, \text{Fe}^{2+})_4\text{Fe}^{3+}\text{Si}_{12}\text{O}_{30}]$ and roedderite $[\text{KNaMg}_2(\text{Mg}_3\text{Si}_{12}\text{O}_{30})]$ are linked by the substitution $\text{Fe}^{3+} + \square \rightleftharpoons \text{Fe}^{2+} + (\text{K} + \text{Na})^+$ and belong to the osumilite (or milarite) group of minerals (Velde *et al.*, 1989; Fleischer and Mandarino, 1991; Hawthorne *et al.*, 1991) with the crystal chemical formula $^{[6]}A_2^{[9]}B_2^{[12]}C^{[18]}D^{[4]}T2_3^{[4]}T1_{12}\text{O}_{30}$ (where: $^{[6]}A = \text{Fe}^{2+}, \text{Fe}^{3+}, \text{Li}, \text{Mg}, \text{Mn}^{2+}, \text{Na}, \text{Sn}, \text{Ti}, \text{Zn}, \text{Zr}$; $^{[9]}B = \text{Na}, \text{H}_2\text{O}, \square, \text{Ca}?, \text{K}?$; $^{[12]}C = \text{K}, \text{Na}, \text{Ca}, \text{Ba}$; $^{[18]}D = \square, ?$; $^{[4]}T2 = \text{Al}, \text{Be}, \text{Fe}^{2+}, \text{Fe}^{3+}, \text{Li}, \text{Mg}$; $^{[4]}T1 = \text{Si}, \text{Al}$), which crystallize in the $P6/mcc$, $P6_2c$ and, probably, $Acam$, $Aba2$ space groups (Armbruster, 1989; Fleischer and Mandarino, 1991). Each $T1$ tetrahedron shares three corners with adjacent $T1$ tetrahedra to form six-membered double rings that are linked each other, laterally and vertically, by sharing the fourth corner with an A octahedron and a $T2$ tetrahedron. $T2$ tetrahedra and A octahedra form edge-sharing 12-membered rings. Along the channels, formed by the $T1$ double rings alternating with the $T2/A$ rings, the C and D

sites occur in twelve and eighteen coordination, respectively. Sandwiched between two adjacent A octahedra are the B sites in octahedral or nine coordination (Abraham *et al.*, 1983; Armbruster and Oberhänsli, 1988a,b; Khan *et al.*, 1972). In the Bragg classification of the silicates, osumilite-type minerals belong to double-ring structures, and to the tetrahedral framework structures if the chemical identity of tetrahedrally coordinated cations is not considered (Zoltai, 1960; Liebau, 1985). Hawthorne and Smith (1986), in a topological approach to the derivation and characterization of four-connected three-dimensional nets for framework silicate structures, assigned the osumilite-type structures to net 279 which consists of six- ($T1$ tetrahedra) and nine-membered ($T1$ and $T2$ tetrahedra) rings, each of which is arranged along the $[001]$ direction to form channels which contain A octahedra, B , C , and D sites (Fig. 1). Hawthorne *et al.* (1991), according to this topological structural model, also discussed the crystal chemistry of the osumilite-type minerals.

Crystal-structure refinement of the Mg-bearing osumilite-type minerals, roedderite, eifelite and

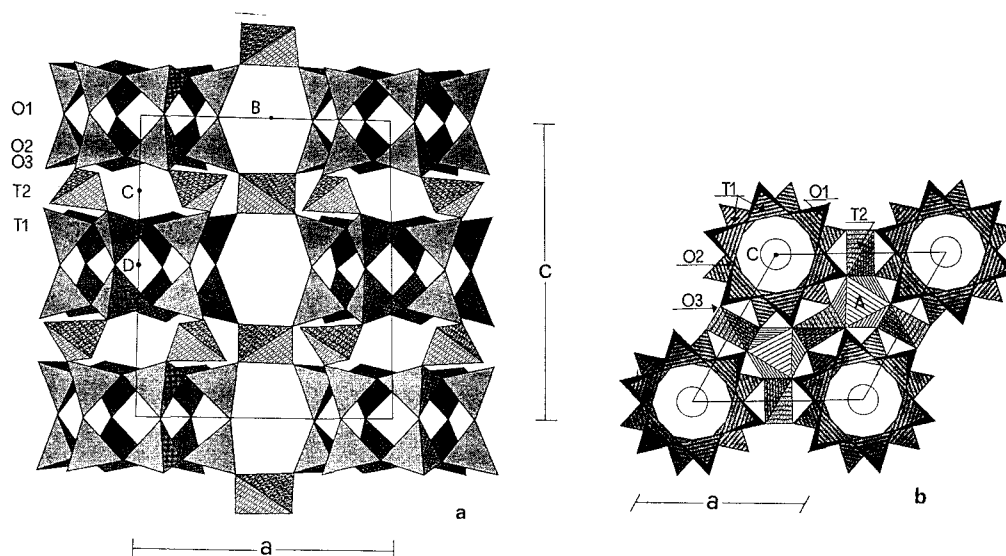


FIG. 1. Polyhedral representation of the osumilite-type structure (a) projected onto (101) and (b) projected onto (001). *A* polyhedra are omitted in the projection onto (101) for clarity.

merrihueite, shows unusual 4-coordination for Mg, which occupies the *T2* site (Abraham *et al.*, 1983; Armbruster, 1989; Khan *et al.*, 1972). Furthermore, in roedderite, the *B* site splits into two different *B* positions: *B1*, preferentially occupied by Na, and *B2*, which is either empty or contains only small amounts of Na; this reduces the symmetry from *P6/mcc* to *P6̄2c* (Armbruster, 1989). The occurrences and the conditions of crystallization of natural and synthetic minerals of the osumilite group have been summarized by Hawthorne *et al.* (1991).

The aim of this work is to characterize the crystal-chemical structure of minerals intermediate in composition between roedderite and chayesite ($0.42 \leq \text{Fe}^{3+} \leq 0.87$ apfu; $0.00 \leq \text{Fe}^{2+} \leq 1.19$ apfu; $0.14 \leq \text{Na} \leq 0.62$ apfu), and to relate the crystal-chemical results to the evolution of the host melts.

Sample description

The samples were collected from the lamproitic outcrop at Sierra de las Cabras, *c.* 0.7 km from Cancarix (Albacete province, SE Spain). The outcrop consists (Contini *et al.*, 1993) of a main central body of holocrystalline, fine-grained, sanidine–K-richterite (with Na-Fe-rich arfvedsonite rims)–olivine–phlogopite–diopside (plus late accessory Na-Fe-clinopyroxene)-rich rocks surrounded by glass-rich lavas.

Roedderite–chayesite (Fig. 2) are accessory minerals in the Cancarix rocks (Wagner and Velde, 1986), associated with Ti-rich (pseudobrookite, rutile) and K-Zr-Ti-rich (dalyite) phases; they occur as anhedral grains and are distinctly pleochroic, colourless to deep blue. Usually, they fill voids (sample SP719); sometimes, they are intergrown with amphibole (sample SP724). The crystallization of roedderite–chayesite minerals therefore occurred contemporaneously with or subsequently to the crystallization of amphibole (K-richterite and/or arfvedsonite rims) at *c.* 1000°C (S. Mariani, pers. comm.). In the lavas surrounding the main body,

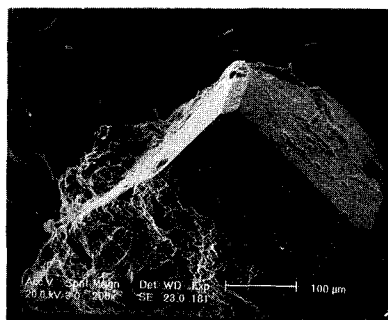


FIG. 2. Scanning electron photomicrograph of a crystal of roedderite–chayesite.

TABLE 1. Representative electron microprobe analyses and chemical formulae of Cancarix roedderite-chayesite

	1	2	3	4	5	6	7	11	13	16	18	24	27	30
Chemical composition (mean of 10 point analyses)														
SiO ₂	70.64	70.80	70.68	71.13	71.13	70.59	70.94	71.21	71.03	69.83	69.80	70.60	68.98	68.75
TiO ₂	0.19	0.23	0.11	0.04	0.06	0.05	0.07	0.11	0.16	0.20	0.18	0.11	0.08	0.20
Al ₂ O ₃	0.27	0.23	0.12	0.32	0.20	0.23	0.34	0.28	0.32	0.21	0.19	0.19	0.15	0.14
Fe ₂ O ₃ *	6.47	4.70	5.36	6.52	5.21	5.31	5.55	5.75	4.78	4.67	3.27	4.39	6.70	5.81
FeO							0.17	0.05	0.99	4.62	3.09	1.99	5.29	8.15
MnO	0.10	0.28	0.03	0.03	0.25	0.25	0.14	0.09	—	0.10	0.10	0.56	0.23	0.33
MgO	16.47	17.22	17.07	16.72	17.13	16.92	16.94	16.96	16.87	14.51	16.05	16.16	12.85	11.45
CaO	0.02	—	0.02	0.02	—	—	0.03	0.02	—	—	0.02	—	—	—
BaO	0.06	—	0.06	0.07	—	—	0.03	—	—	0.06	—	—	—	—
Na ₂ O	0.62	1.68	0.92	0.90	1.83	1.90	1.26	1.13	1.41	1.34	1.78	1.39	0.43	0.69
K ₂ O	4.18	4.13	4.31	3.99	3.71	3.70	4.42	4.40	4.40	4.31	4.57	4.61	4.50	4.47
Sum	99.02	99.27	98.68	99.74	99.52	98.95	99.89	100.00	99.96	99.85	99.05	100.00	99.21	99.99
Structural formulae on the basis of 30 oxygens														
Si	11.95	11.95	11.98	11.94	11.96	11.95	11.93	11.94	11.94	11.96	11.96	11.96	11.97	11.97
Al	0.05	0.05	0.02	0.06	0.04	0.05	0.07	0.06	0.06	0.04	0.04	0.04	0.03	0.03
Sum	12.00	12.00	12.00	12.00	12.00	12.00	12.00	12.00	12.00	12.00	12.00	12.00	12.00	12.00
Ti	0.02	0.03	0.01	—	0.01	0.01	0.01	0.01	0.02	0.03	0.02	0.01	0.01	0.03
Fe ³⁺	0.82	0.60	0.68	0.82	0.66	0.68	0.70	0.73	0.61	0.60	0.42	0.56	0.87	0.76
Fe ²⁺							0.02	0.01	0.14	0.66	0.44	0.28	0.77	1.19
Mn	0.01	0.04	—	—	0.04	0.04	0.02	0.01	—	0.01	0.02	0.08	0.03	0.05
Mg	4.15	4.33	4.31	4.18	4.29	4.27	4.25	4.24	4.23	3.70	4.10	4.07	3.32	2.97
Sum	5.00	5.00	5.00	5.00	5.00	5.00	5.00	5.00	5.00	5.00	5.00	5.00	5.00	5.00
m.a.n.	71.81	69.22	69.62	71.48	69.86	70.14								
Na	0.20	0.55	0.30	0.29	0.60	0.62	0.41	0.37	0.46	0.44	0.59	0.46	0.14	0.23
K	0.90	0.89	0.93	0.85	0.80	0.80	0.95	0.94	0.94	0.94	1.00	1.00	1.00	0.99
Sum	1.10	1.44	1.23	1.14	1.40	1.42	1.37†	1.31	1.40	1.38	1.59	1.46	1.14	1.22
m.a.n.	19.30	22.96	20.97	19.34	21.80	22.02								
m.a.n. for structural sites based on X-ray refinement														
T2	42.30	44.40	43.32	44.40	44.40	45.06								
A	29.60	24.80	26.34	27.07	25.41	25.12								
T2 + A	71.90	69.20	69.66	71.47	69.81	70.18								
C	18.19	18.11	18.41	17.73	17.37	17.37								
B	1.13	4.90	2.46	1.47	4.36	4.62								
C + B	19.32	23.01	20.87	19.20	21.73	21.99								

Note: * For method of calculation see text; † Ca = 0.01. Analyses 1–6 refer to the same crystals used in the structure refinement; analyses 7–30 refer to crystals analysed in thin-section; analyses 1–13 refer to crystals in rock sample SP719; analyses 16–30 to crystals in rock sample SP724. m.a.n. = mean atomic number.

roedderite and chayesite are very rare and occur as anhedral-subhedral crystals which are colourless to weakly pleochroic (light blue tint, uniaxial positive) filling cavities and vugs.

Experimental

The average chemical compositions (ARL-SEMQ electron microprobe analysis of polished thin-sections and of crystals used for structure

refinement, Table 1) are representative of each entire crystal. H₂O was determined on selected crystals by thermal analysis (DTA, TG, DTG) using a SEIKO SSC/5200 apparatus (temperature rate: 10°/min in the range T_{amb} –1000°C under argon flow).

Crystals examined preliminarily by precession photographs have hexagonal symmetry with hhl , $hh\bar{l}$, $h0l$ present only with $l = 2n$. The crystals with the highest iron content ($Fe^{3+} > 0.82$ apfu)

TABLE 2. Lattice constants and some crystallographic data of roedderite-chayesite crystals studied

Sample	dimensions (mm)	s.m.,w.	N_{obs}	R_{sym}	R_{all}	R_{obs}	h.m.r.	a [Å]*	c [Å]*	Vol.[Å ³]*
1	0.12 × 0.15 × 0.15	ω, 1.50	538	0.022	0.029	0.026	0.57	10.118 (1)	14.300 (3)	1267.8
2	0.21 × 0.22 × 0.22	ω, 1.20	694	0.013	0.028	0.026	0.33	10.124 (1)	14.305 (1)	1269.8
3	0.17 × 0.22 × 0.24	ω, 1.20	612	0.018	0.026	0.025	0.35	10.122 (2)	14.320 (2)	1270.6
4	0.12 × 0.17 × 0.17	ω, 1.00	657	0.017	0.023	0.021	0.32	10.128 (1)	14.312 (1)	1271.4
5	0.12 × 0.12 × 0.14	ω, 0.80	596	0.016	0.023	0.021	0.37	10.135 (1)	14.320 (1)	1273.9
6	0.11 × 0.12 × 0.21	ω, 0.90	658	0.015	0.021	0.020	0.36	10.126 (1)	14.326 (1)	1272.1

Note: Esd's on the last significant digit are in parentheses;

s.m.,w: scan mode, width [°]

$$R_{\text{sym}} = \frac{\sum_{hkl} \sum_{i=1}^N |I_{hkl,i} - \bar{I}_{hkl}|}{\sum_{hkl} \sum_{i=1}^N I_{hkl,i}};$$

h.m.r.: highest map residual (e⁻/Å³);

* determined on 25 reflections (25° ≤ 2θ ≤ 50°).

are unsuitable for structural investigation. Intensity data (4° ≤ 2θ ≤ 66°) were collected with an ENRAF-NONIUS CAD4 automated four-circle diffractometer operating at 52 kV and 40 mA with graphite-monochromated Mo-Kα X-ray radiation. Unit cell dimensions and additional information on X-ray data measurement and structure refinement are reported in Table 2. Absorption corrections were applied according to the semi-empirical method of North *et al.* (1968). Data were corrected for Lorentz-polarization and background effects then averaged and reduced to structure factors. The refined coordinates for osumilite (Armbruster and Oberhänsli, 1988a) were used as input to the least-squares program of the system SHELX-76 (Sheldrick, 1976). Subsequent difference-Fourier maps indicated residual density at 1/4, 3/4, 0 assigned to the *B* site. Upon conversion to an anisotropic displacement model, the displacement model of the *B* site showed unreasonably large anisotropy in three crystals (2, 5, 6). This was taken as evidence for positional disorder of the *B*-cation. The electron density was modelled as a split site with an isotropic displacement factor. Crystal-structure refinement does not indicate ordering into *B* sites in *P*6̄2c, and we prefer the space group *P*6/*mcc*. We used scattering factors for ionized Fe, Mg, K and Na, and mixed scattering factors (in the ratio 1:1) for tetrahedral *T*1 and anion sites. Cycles of least-squares refinement with anisotropic displacement parameters, variable occupancy of K vs. Na and Fe vs. Mg, converged to the final positional and anisotropic parameters listed in Table 3. Table 4 lists the selected bond-lengths, angles and distortion parameters. A supplementary Table of observed and calculated structure factors is available from the editor on request.

Crystal chemistry

The samples studied are unzoned, but the compositions of crystals from the same rock sample are variable (Table 1). The main chemical variations involve the Fe_{tot}/Mg ratio (0.138 to 0.656), which is highest in the chayesite intergrown with amphibole (sample SP724), and the Na/K ratio (0.140 to 0.775), and compositions plot close to the solid-solution line Fe³⁺ + □ ⇌ Fe²⁺ + (K+Na)⁺ (Fig. 3) that links the two ideal end-members.

*T*1 tetrahedron. The <*T*1–O> bond-lengths (1.609 ≤ <*T*1–O> ≤ 1.611 Å) suggest constant occupancy of the *T*1 site. In particular, microprobe chemical analyses (samples 1–6) have an average Si content of 11.96 apfu, close to the number (12) of *T*1 sites corresponding to the structural formula. Hawthorne *et al.* (1991) found a predictive relationship between tetrahedral <*T*1–O> bond-lengths and Al content [i.e. <*T*1–O> = 1.609 + 1.0(*r*_{*T*1}), where *r*_{*T*1} is the mean radius of the *T*1 cations]. Our samples conform to the linear relationship and plot close to milarite, which represents the Si-rich end-member (Fig. 4).

*T*2 tetrahedron. The *T*2 tetrahedron is large (1.934 ≤ *T*2–O ≤ 1.941 Å) and extremely distorted indicating that Mg occupies the *T*2 site. The *T*2–O bond-length is a little shorter (eifelite: *T*2–O = 1.989 Å; merrihueite: *T*2–O = 1.955 Å) and the scattering is slightly higher than would be expected if the site was occupied only by Mg; thus we conclude that some Fe³⁺ also occurs at the *T*2 site. *T*2–O bond-length could be also affected by the size of the *A* octahedron and by the *B* position and occupancy (Hawthorne *et al.*, 1991). In samples which show the *B* site at *z* = 0, the

TABLE 3. Atom coordinates and displacement factors [\AA^2] for roedderite-chayesite crystals

Atom	x/a	y/b	z/c	B_{eq}	β_{11}^*	β_{22}^*	β_{33}^*	β_{12}^*	β_{13}^*	β_{23}^*
Sample 1										
O1	0.1298(3)	0.3948(3)	0	1.76(9)	2.3(1)	2.1(1)	1.01(9)	1.1(1)	0	0
O2	0.2195(2)	0.2776(2)	0.1332(1)	1.58(7)	1.54(7)	1.87(7)	1.63(7)	1.07(6)	0.01(6)	-0.06(6)
O3	0.1545(2)	0.4964(2)	0.1725(1)	1.25(6)	1.19(6)	1.32(6)	1.22(6)	0.61(5)	-0.10(6)	-0.18(6)
T1	0.23840(7)	0.35292(7)	0.39072(4)	0.92(2)	0.94(2)	1.06(2)	0.84(2)	0.56(2)	0.05(2)	0.05(2)
T2	½	½	¼	0.86(5)	0.60(4)	1.52(9)	0.77(5)	0.76(4)	0	0
A	½	¾	¼	1.82(4)	1.73(4)	1.73(4)	2.00(8)	0.87(2)	0	0
C	0	0	¼	2.04(5)	2.02(5)	2.02(5)	2.1(1)	1.01(3)	0	0
B	½	¾	0	1.2(5)	-	-	-	-	-	-
Sample 2										
O1	0.1299(2)	0.3945(2)	0	1.91(6)	2.35(8)	1.93(7)	1.37(7)	1.02(7)	0	0
O2	0.2193(1)	0.2776(1)	0.13327(9)	1.73(5)	1.67(5)	1.96(5)	1.95(5)	1.21(4)	-0.04(4)	0.02(4)
O3	0.1550(1)	0.4966(1)	0.17245(8)	1.34(4)	1.23(4)	1.34(4)	1.45(4)	0.64(3)	-0.08(4)	-0.19(4)
T1	0.23814(5)	0.35274(5)	0.39066(3)	0.99(1)	0.94(2)	1.02(2)	1.09(2)	0.53(1)	0.04(1)	0.06(1)
T2	½	½	¼	1.10(3)	0.78(3)	1.72(6)	1.12(3)	0.86(3)	0	0
A	½	¾	¼	1.03(3)	0.95(3)	0.95(3)	1.18(6)	0.48(2)	0	0
C	0	0	¼	2.10(4)	1.98(4)	1.98(4)	2.34(7)	0.99(2)	0	0
B	½	¾	-0.0202(7)	1.7(2)	-	-	-	-	-	-
Sample 3										
O1	0.1297(2)	0.3938(2)	0	1.85(7)	2.21(9)	2.12(9)	1.25(7)	1.10(8)	0	0
O2	0.2194(2)	0.2777(2)	0.1334(1)	1.74(5)	1.68(5)	2.04(6)	1.94(6)	1.27(5)	0.00(5)	0.03(5)
O3	0.1549(1)	0.4965(2)	0.17246(9)	1.38(5)	1.22(5)	1.34(5)	1.57(5)	0.64(4)	-0.09(4)	-0.17(5)
T1	0.23828(5)	0.35296(5)	0.39076(4)	1.07(2)	0.95(2)	1.07(2)	1.25(2)	0.55(1)	0.03(2)	0.06(2)
T2	½	½	¼	1.09(4)	0.70(3)	1.67(7)	1.22(4)	0.84(3)	0	0
A	½	¾	¼	1.26(4)	1.26(3)	1.22(3)	1.63(6)	0.84(3)	0	0
C	0	0	¼	1.84(5)	1.62(5)	1.62(5)	2.27(9)	0.81(2)	0	0
B	½	¾	0	2.0(3)	-	-	-	-	-	-
Sample 4										
O1	0.1304(2)	0.3947(2)	0	1.63(6)	1.95(8)	1.55(7)	1.39(7)	0.87(6)	0	0
O2	0.2198(1)	0.2781(1)	0.13350(8)	1.49(4)	1.36(5)	1.68(5)	1.82(5)	1.05(4)	0(4)	-0.01(4)
O3	0.1553(1)	0.4971(1)	0.17254(8)	1.07(4)	0.90(4)	0.95(4)	1.33(4)	0.45(3)	-0.12(3)	-0.24(4)
T1	0.23803(5)	0.35318(4)	0.39069(3)	0.78(1)	0.66(1)	0.75(1)	0.99(2)	0.40(1)	0.06(1)	0.08(1)
T2	½	½	¼	0.89(3)	0.53(3)	1.44(6)	1.00(3)	0.72(3)	0	0
A	½	¾	¼	0.89(2)	0.71(2)	0.71(2)	1.24(5)	0.36(1)	0	0
C	0	0	¼	1.76(3)	1.60(3)	1.60(3)	2.07(6)	0.80(2)	0	0
B	½	¾	0	0.8(4)	-	-	-	-	-	-
Sample 5										
O1	0.1299(2)	0.3943(2)	0.0	1.66(7)	2.25(9)	1.81(8)	0.90(7)	1.00(8)	0	0
O2	0.2197(2)	0.2777(2)	0.13325(9)	1.50(5)	1.56(5)	1.77(5)	1.56(5)	1.11(5)	0.04(5)	0.05(5)
O3	0.1552(1)	0.4967(1)	0.17230(8)	1.10(4)	1.04(5)	1.13(4)	1.10(4)	0.53(4)	-0.08(4)	-0.18(4)
T1	0.23807(5)	0.35288(5)	0.39065(3)	0.80(2)	0.84(2)	0.92(2)	0.72(2)	0.49(1)	0.05(2)	0.07(2)
T2	½	½	¼	0.83(3)	0.59(3)	1.56(7)	0.66(3)	0.78(3)	0	0
A	½	¾	¼	0.84(3)	0.80(3)	0.80(3)	0.93(5)	0.40(2)	0	0
C	0	0	¼	1.64(4)	1.55(4)	1.55(4)	1.80(7)	0.78(2)	0	0
B	½	¾	-0.0188(8)	1.0(2)	-	-	-	-	-	-
Sample 6										
O1	0.1299(2)	0.3943(2)	0	1.61(5)	2.14(8)	1.73(7)	0.95(6)	0.96(6)	0	0
O2	0.2197(1)	0.2778(1)	0.13331(8)	1.46(4)	1.44(5)	1.74(5)	1.62(4)	1.10(4)	-0.01(4)	0.02(4)
O3	0.1551(1)	0.4967(1)	0.17248(7)	1.07(4)	1.04(4)	1.07(4)	1.09(4)	0.53(3)	-0.10(3)	-0.23(4)
T1	0.23814(4)	0.35284(4)	0.39067(3)	0.77(1)	0.79(1)	0.87(1)	0.72(1)	0.46(1)	0.05(1)	0.07(1)
T2	½	½	¼	0.85(3)	0.59(3)	1.57(6)	0.72(3)	0.78(3)	0	0
A	½	¾	¼	0.76(3)	0.71(3)	0.71(3)	0.85(5)	0.36(2)	0	0
C	0	0	¼	1.61(3)	1.54(3)	1.54(3)	1.76(6)	0.77(2)	0	0
B	½	¾	-0.0190(7)	1.5(2)	-	-	-	-	-	-

Note: Esd's on the last significant digit are in parentheses;

* the form of the anisotropic thermal parameter is: $\exp[-\frac{1}{4}(B_{11}h^2a^{*2} + B_{22}k^2b^{*2} + B_{33}l^2c^{*2} + 2B_{12}hka^*b^* + 2B_{13}hla^*c^* + 2B_{23}klb^*c^*)]$.

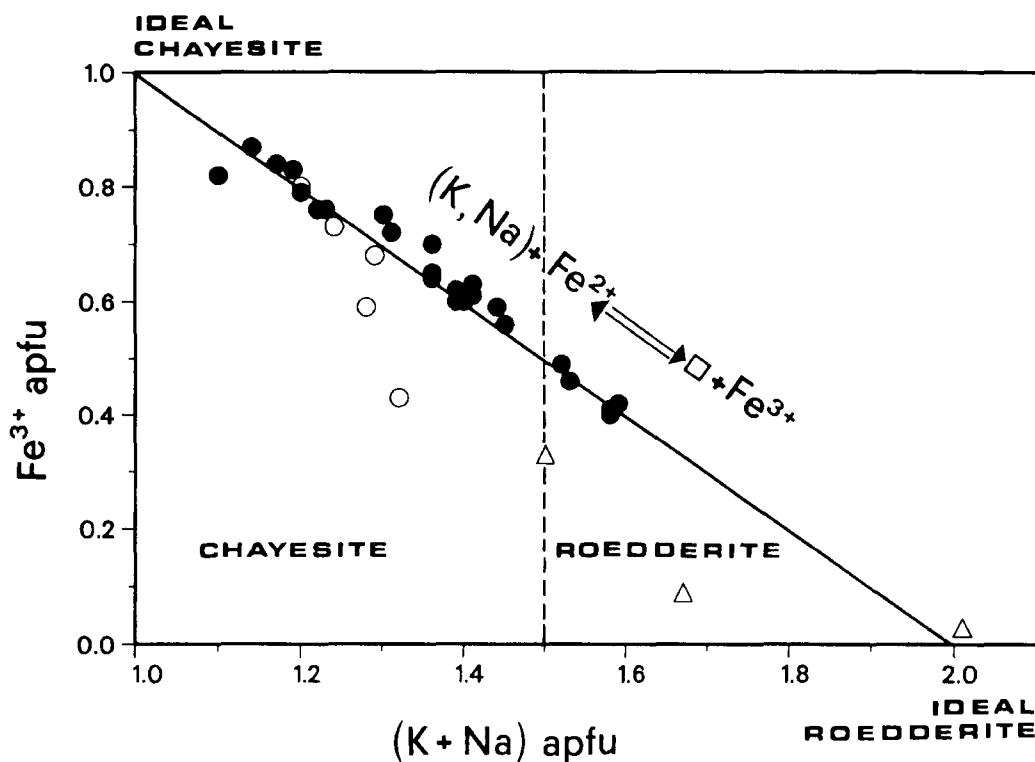


FIG. 3. Plot of calculated Fe^{3+} content (apfu) vs. $(\text{Na} + \text{K})$ content (apfu). Filled circles: samples from this study; open circles: chayesites from Moon Canyon (Velde *et al.*, 1989); triangles: Bellerberg roedderites (Abraham *et al.*, 1983). The points reported in the plot refer to all analysed crystals. Ideal roedderite: $\text{KNaMg}_3\text{Si}_{12}\text{O}_{30}$; ideal chayesite: $\text{K}(\text{Mg}, \text{Fe}^{2+})_4\text{Fe}^{3+}\text{Si}_{12}\text{O}_{30}$.

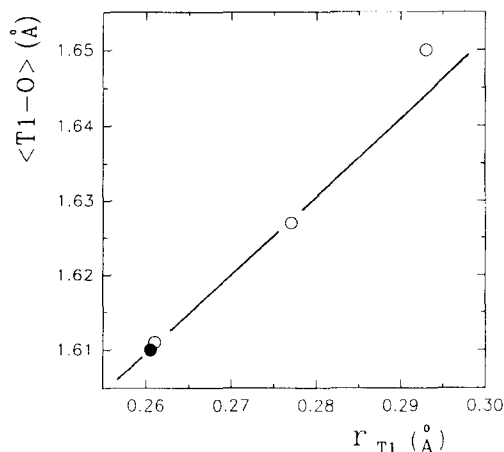


FIG. 4. Plot of $\langle \text{T1-O} \rangle$ [Å] vs. cation radius [Å] at the T1 site. The filled circle is the mean data of the studied samples; the open circles are the mean values of the data for milarite, osumilite and armenite reported by Hawthorne *et al.* (1991) as well as the straight line.

observed small increase in T2-O vs. T2 occupancy can be attributed to the presence of large cations (e.g. Fe^{2+} , Mn^{2+}) as well (Tables 1 and 4).

A, B, and C polyhedra. Site-occupancy refinement indicates small amounts of iron in the A octahedron; the A-O bond-lengths, indicate this iron to be in the trivalent state. The population of the C site consists of K with small amounts of Na ($0.10 \leq \text{Na} \leq 0.20$ apfu). The incorporation of alkaline cations (Na) in the ideally empty B (or B') polyhedron is the charge compensation mechanism for the incorporation of Mg at T2 in excess of the ideal amount $\text{Fe}^{3+}:\text{Mg}^{2+} = 1:2$.

In all samples, difference-Fourier maps show maxima ($2.0 \leq e^{-}/\text{Å}^3 \leq 4.0$) close to $\frac{1}{3}, \frac{2}{3}, 0$ (site symmetry 6). Therefore, samples 2, 5 and 6, with Na at $\frac{1}{3}, \frac{2}{3}, 0$, had a large displacement parameter along the *c* axis, suggesting that Na is disordered at positions of the type $\frac{1}{3}, \frac{2}{3}, z$ (site symmetry 3, with $-0.020 \leq z \leq -0.018$), with Na showing distorted ninefold coordination. The refined scattering at the B site is in good agreement with

TABLE 4. Selected bond-lengths and angles from structure refinement of roedderite-chayesite crystals

	1	2	3	4	5	6
C-O2 [$\times 12$]	3.062(1)	3.062(1)	3.062(1)	3.066(1)	3.067(1)	3.066(1)
B-O1 [$\times 3$]	2.478(2)	2.498(2)	2.487(2)	2.480(1)	2.501(2)	2.499(2)
B-O3 [$\times 6$] ([$\times 3$])	3.034(2)	3.273(9)	3.036(1)	3.033(1)	3.257(9)	3.262(9)
B-O3' ([$\times 3$])	-	2.803(8)	-	-	2.819(9)	2.819(8)
<B-O>	2.849	2.858	2.853	2.849	2.859	2.860
A-O3 [$\times 6$]	2.087(1)	2.085(1)	2.086(1)	2.079(1)	2.087(1)	2.085(1)
O3-O3 [$\times 3$]	2.917(3)	2.914(3)	2.916(3)	2.912(3)	2.918(3)	2.916(2)
O3-O3 [$\times 3$]	2.757(3)	2.758(3)	2.760(3)	2.753(2)	2.765(3)	2.760(2)
O3-O3 [$\times 6$]	3.062(2)	3.057(2)	3.058(2)	3.051(2)	3.058(2)	3.057(2)
<O-O>	2.950	2.947	2.948	2.942	2.950	2.948
T2-O3 [$\times 4$]	1.932(2)	1.936(1)	1.936(2)	1.937(1)	1.941(2)	1.937(1)
O3-O3 [$\times 2$]	3.500(3)	3.509(2)	3.509(3)	3.513(2)	3.518(2)	3.511(2)
O3-O3 [$\times 2$]	2.757(3)	2.758(3)	2.760(3)	2.753(2)	2.765(3)	2.760(2)
O3-O3 [$\times 2$]	3.164(4)	3.173(3)	3.172(3)	3.177(3)	3.181(3)	3.175(3)
<O-O>	3.140	3.147	3.147	3.148	3.155	3.149
O3-T2-O3 [$\times 2$]	129.9(1)	129.97(7)	129.93(9)	130.16(7)	129.99(8)	129.99(7)
O3-T2-O3 [$\times 2$]	91.02(8)	90.82(6)	90.91(7)	90.59(6)	90.83(6)	90.84(5)
O3-T2-O3 [$\times 2$]	109.9(1)	110.08(7)	110.01(8)	110.17(7)	110.05(8)	110.04(7)
<O-T2-O>	110.27	110.29	110.28	110.31	110.29	110.29
TAV _{T2}	303.2	307.4	305.4	314.0	307.6	307.4
T1-O1	1.606(1)	1.607(1)	1.606(1)	1.607(1)	1.609(1)	1.609(1)
T1-O2	1.622(2)	1.621(1)	1.623(2)	1.621(2)	1.624(2)	1.623(2)
T1-O2'	1.624(2)	1.625(1)	1.626(2)	1.630(2)	1.626(2)	1.624(2)
T1-O3	1.582(2)	1.584(1)	1.583(2)	1.586(1)	1.583(1)	1.585(1)
<T1-O>	1.609	1.609	1.610	1.611	1.611	1.610
O1-O2	2.649(2)	2.652(2)	2.651(2)	2.656(2)	2.652(2)	2.652(2)
O1-O2	2.633(3)	2.632(2)	2.631(3)	2.634(2)	2.632(3)	2.634(2)
O1-O3	2.635(2)	2.637(1)	2.642(2)	2.641(1)	2.639(1)	2.642(1)
O2-O2	2.566(1)	2.567(1)	2.567(1)	2.572(1)	2.572(1)	2.570(1)
O2-O3	2.601(2)	2.607(2)	2.604(2)	2.608(2)	2.607(2)	2.605(2)
O2-O3	2.665(3)	2.665(2)	2.663(3)	2.666(2)	2.667(2)	2.665(2)
<O-O>	2.625	2.627	2.626	2.630	2.628	2.628
O1-T1-O2	110.2(1)	110.23(7)	110.21(9)	110.26(7)	110.12(8)	110.19(7)
O2-T1-O1	109.2(1)	109.2(1)	109.2(1)	109.3(1)	109.2(1)	109.18(8)
O1-T1-O3	111.5(1)	111.46(8)	111.9(1)	111.59(8)	111.54(9)	111.66(8)
O2-T1-O2	104.5(1)	104.53(8)	104.41(8)	104.61(7)	104.62(8)	104.6(7)
O2-T1-O3	108.58(8)	108.66(6)	108.50(7)	108.39(6)	108.66(7)	108.52(6)
O3-T1-O2	112.5(1)	112.49(7)	112.36(8)	112.44(7)	112.51(8)	112.41(7)
<O-T1-O>	109.41	109.43	109.43	109.43	109.44	109.43
TAV _{T1}	7.97	7.76	8.38	7.81	7.64	7.73

Note: Esd's on the last significant digit are in parentheses;
TAV as in Robinson *et al.* (1971).

the excess Na given by chemical analysis. It is worth noting that the samples analysed are anhydrous, which excludes any effect of water on the displacement of the B site along the *c* axis, as is the case in milarite (Hawthorne *et al.*, 1991).

Concluding remarks

Minerals of the chayesite-roedderite series from Cancarix lamproites have variable chemistry characterized by the substitution $\text{Fe}^{3+} + \square \rightleftharpoons \text{Fe}^{2+} + (\text{K} + \text{Na})^+$, trending from chayesite to

roedderite with progressive crystallization. Crystallization of olivine and (subordinately) clinopyroxene, phlogopite and sanidine led to the progressive increase in Fe/Mg and Na/K of the solidifying melts. In particular, the Na/K ratio reached its peak with the separation of the arfvedsonitic rims, and then decreased from the early- to the later-crystallized grains of chayesite-like phases (Na/K ratios 0.6 and 0.1, respectively). Thus, the crystallization of the roedderite-type minerals, with Na/K substitution at the C site and/or very low Na occupancy at the B site, record the

